
Article:
Shanshal, A., Hoang, K. orcid.org/0000-0001-7463-9681 and Atallah, K. orcid.org/0000-0002-8008-8457 (2019) High-performance ferrite permanent magnet brushless machines. IEEE Transactions on Magnetics, 55 (7). 8104504. ISSN 0018-9464

https://doi.org/10.1109/tmag.2019.2900561

High performance Ferrite permanent magnet brushless machines

Abdullah Shanshal, Khoa Hoang and Kais Atallah

Department of Electronic and Electrical Engineering, the University of Sheffield, Sheffield, UK

Abstract— the performance of a brushless permanent magnet machine topology equipped with axially and circumferentially magnetised ferrite permanent magnets is presented. Simulation studies show that for smaller ratios of axial length to active length, airgap flux densities in excess of 1T can be achieved, resulting in significant improvements, in torque production and efficiency. A prototype machine is manufactured and test results confirm the predictions of the EMF and static torque.

Index Terms— Brushless machines, permanent magnets.

I. INTRODUCTION

The motivation to reduce or eliminate the use of rare-earth permanent magnets has increased in recent years. This has been due to significant fluctuations in prices and the potential restrictions on future supply [1]. Electrical motors and generators account for more than a third of the current usage of rare-earth permanent magnets [2]. Therefore, permanent magnet free machine topologies, such switched reluctance and induction types [3], and those employing ferrite permanent magnets, are being seriously considered as alternatives in many applications where rare-earth permanent magnet machines would normally be leading candidates, because of their inherent power density and efficiency advantages. These applications include automotive applications, in particular electric and hybrid vehicles, and wind power generation where a direct-drive generator may require more than 500kg of rare-earth permanent magnets per Megawatt rating.

Spoke-type rotors exhibit flux focusing geometries resulting in larger airgap flux densities [4, 5], especially when large numbers of poles are adopted. These topologies may enable the use of cost effective ferrite permanent magnets in order to achieve torque densities and efficiencies close to those of machines employing rare-earth permanent magnets.

The paper describes a permanent magnet brushless machine topology, Fig. 1, employing a rotor [6], equipped with circumferentially and axially magnetised permanent magnets. The fluxes produced by all the permanent magnets are focused in order to achieve airgap flux densities larger than those achievable in conventional spoke-type rotor topologies. Especially, when a lower number of poles may be required. However, the ratio of rotor diameter to active length should be relatively small in order to maximize these advantages.

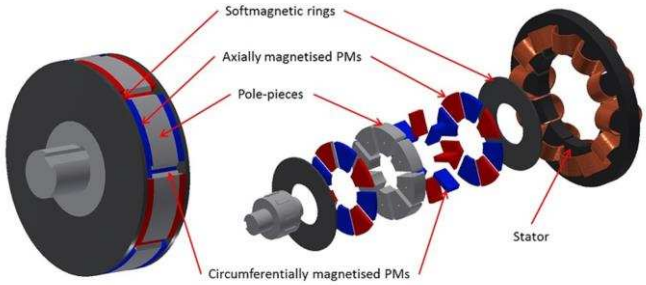

Fig. 1 Schematic of brushless permanent magnet machine with a rotor equipped axially and circumferentially magnetised ferrite permanent magnets.

II. MAGNETIC ANALYSIS

Table 1 gives the parameters of a Ferrite brushless permanent magnet machine, which is equipped with SiFe laminations in the stator, and solid mild steel rings, which offer good magnetic and mechanical properties. The softmagnetic pole-pieces, however, are assumed to be soft magnetic composite, which exhibits an isotropic permeability in all directions, axial, circumferential and radial, while minimizing the likely eddy current losses caused by airgap permeance variations due stator slotting. Due to the nature of the rotor magnetic circuit, 3-dimensional finite analysis is employed, and Fig. 2 shows the variation of the radial component of flux density in the airgap, where it can be seen that an airgap flux density in excess of 1 T can be achieved.

III. PERFORMANCE EVALUATION

For the rotor topology shown in figure 1, which is equipped with axially and circumferentially magnetised permanent magnets, the winding inductances will vary with the rotor position and therefore, a reluctance torque would be produced, if a direct current component is injected. However, the addition of the softmagnetic rings would affect the armature flux paths, and the values of the direct and quadrature inductances, which are likely to exhibit a non-linear relationship with the winding currents.

Table I Parameters of the Ferrite permanent magnet machine

Parameter	Value
Stator active axial length	30 mm
Airgap diameter	200 mm
Stator active diameter	350 mm
Number of pole-pairs	4
Rotor inner active diameter	199 mm
Axial permanent magnet length	7.5 mm
Circumferential permanent magnet length	11.7 mm
Softmagnetic ring axial length	5 mm
Pole-piece to pitch ratio	0.85
Number of slots	12
Slot opening to slot pitch ratio	0.1
Airgap length	0.5 mm
Stator laminations	0.35 mm SiFe
Softmagnetic rings	mild steel
Pole-pieces	SMC
Remanence of permanent magnets B_r	0.39 T
Relative permeability μ_r	1.2
Winding packing factor	0.4
Winding insulation class	F
Ambient temperature	45 °C
Base speed	2250 rpm
Maximum speed	4500 rpm

Under brushless ac operation, the electromagnetic torque resulting from the interaction of rotor permanent magnets and the windings is given by:

$$T_m = \frac{\pi}{2\sqrt{2}}\, k_w\, D_s^2\, l_a\, Q_{rms}\, B_1\, cos(\gamma) \qquad (1)$$

Where D_s is the stator bore diameter, B_1 is the peak fundamental airgap flux density, l_a is the active length, Q_{rms} is the rms electric loading, k_w is the winding factor and γ the advance angle. At the rated current of $I_{rated} = 26.0\ A_{rms}$, the electromagnetic torque produced by the magnets is $T_m = 37.3$ Nm. At base speed, for the rated value of the phase current, a maximum electromagnetic torque $T_e = 38.6$ Nm, can be produced at an advance angle $\gamma = 25^o$. Thus, only 3.5% increase in torque can be achieved through the utilisation of the reluctance component. On the other hand, at maximum speed and rated current, a maximum electromagnetic torque $T_e = 22.3$ Nm is produced at $\gamma = 62.1^o$, with the contribution from the magnets being approximately $T_m = 17.5$ Nm. Fig. 3 shows the variation of torque and power with speed at the rated current $I_{rated} = 26.0\ A_{rms}$. Fig. 4 shows the variation of the electromagnetic torque at rated current with rotor position at base and maximum speeds, where it can be seen that 6th and 12th are the dominant ripple harmonics, especially at maximum speed, where the contribution from the reluctance torque is more significant. Fig. 5 shows the predicted efficiency map, where it can be seen that efficiencies in excess of 97% can be achieved.

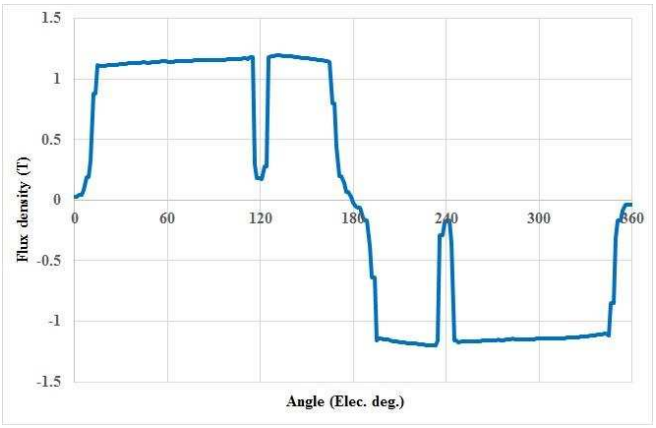

(b) Waveform

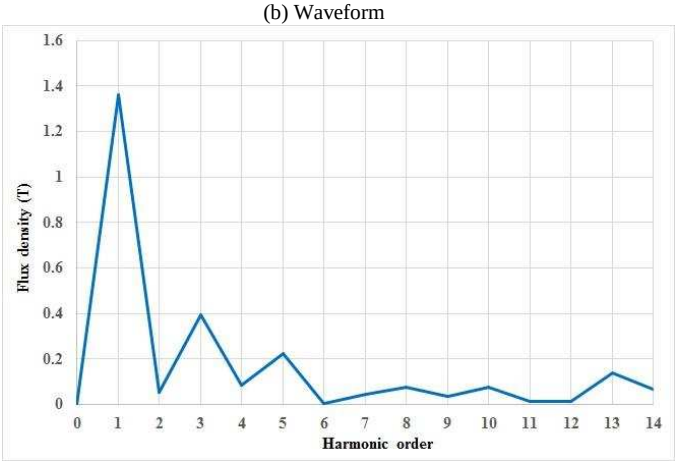

(b) Harmonic spectrum

Fig. 2 Airgap flux density waveform

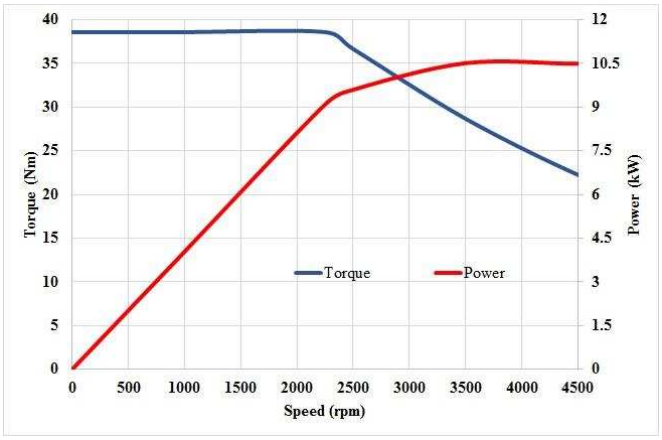

Fig. 3 Variation of torque and power with speed at rated current

The assessment of demagnetisation withstand is an important design step for any PM machine, being more pressing for Ferrite PM brushless machines, due to the inherently lower coercivity of Ferrite PMs, particularly at low temperatures. The BH characteristic at different temperatures of Ferrite material employed by the machine is given in Fig. 6, whilst Fig. 7 gives the average operating magnetic fields in the circumferential and axial magnets for different operating conditions and different temperatures. It can be seen that for this particular design the risk of demagnetisation is relatively low.

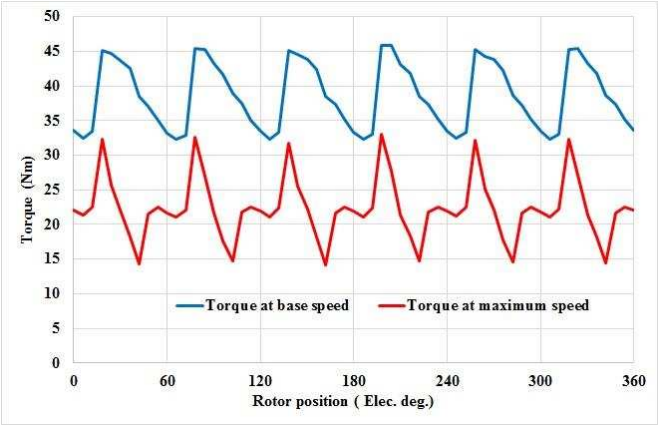

(a) Torque waveforms

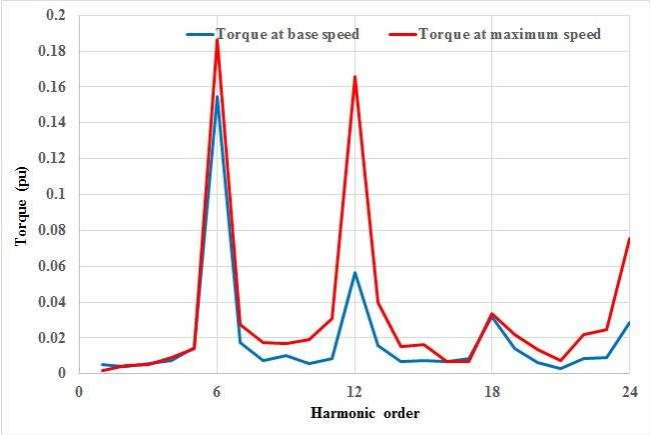

(b) Harmonic spectrum as per unit of corresponding average torque.

Fig. 4 Electromagnetic torque for rated current at base and maximum speeds.

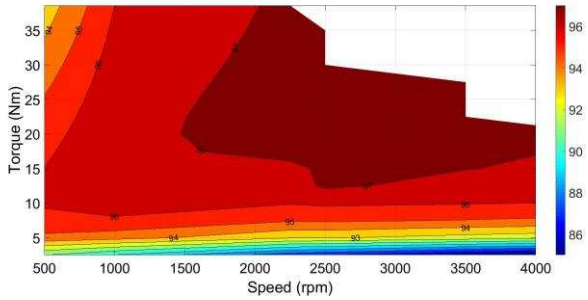

Fig. 5 Efficiency map

IV. Experimental Investigation

A prototype PM machine whose parameters are given in Table 1 has been manufactured and tested, and due to cost constraints and practical difficulties, the axial PMs are realised using a number of rectangular shaped smaller PMs, instead of the ideal geometry adopted in the modelling and analysis in sections II and III. This resulted in ~18% reduction in material used for the axial PMs. Fig. 8 shows the axial PMs, the rotor assembly and the prototype machine during the measurement of the static torque. Fig. 9 compares measured and predicted back EMFs, where it can be seen that good agreement exists. For the static torque measurement, phase A is connected to the

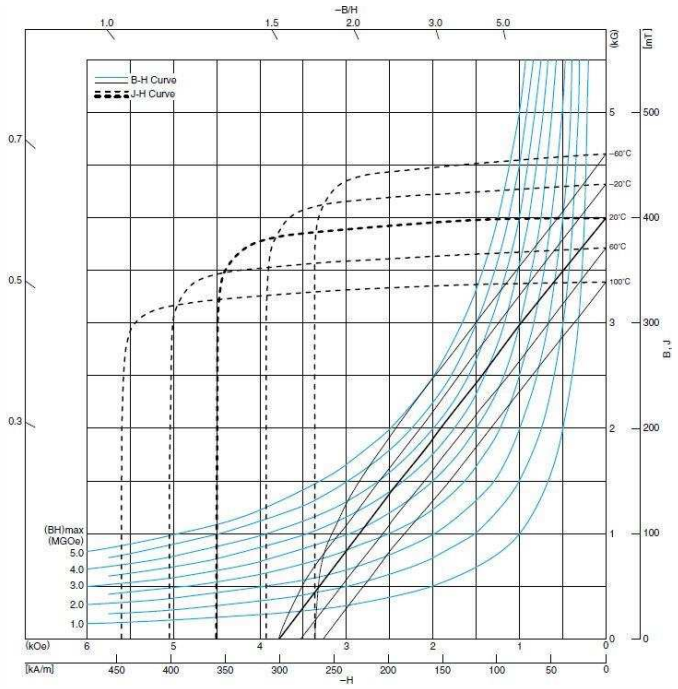

Fig. 6 B-H characteristic of Ferrite material at different temperatures [7]

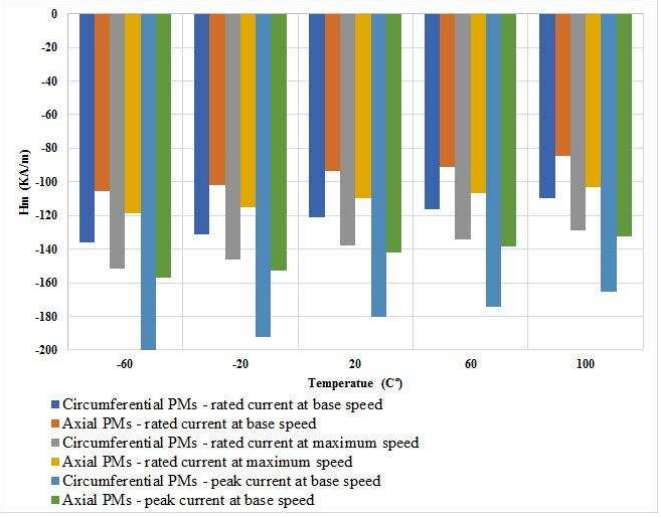

Fig. 7 Magnetic field in the PMs at different operating conditions and different temperatures.

positive terminal of the power supply whilst phases B and C are both connected to the negative terminal. A DC current is then injected. The stator is mounted on the chuck of a lathe which is free to rotate, while the rotor is reacting on precision scales through a balanced beam with a known length. Fig. 10 compares the measured and predicted static torque waveforms where it can be seen that relatively good agreement exists, particularly for the mean values.

V. Conclusions

The performance of a brushless permanent magnet machine topology with a rotor equipped with axially and circumferentially magnetised ferrite permanent magnets in order to achieve airgap flux densities similar to those encountered in rare-earth PM machines is presented. It has been

shown that airgap flux densities in excess of 1 Tesla can be achieved. It has also been shown that the proposed machine topology can exhibit high efficiencies over a wide range of operating conditions. Tests on a prototype machine are presented and it is shown that good agreement between measured and predicted EMF waveforms and static torques exists. Thus, brushless machines employing circumferentially and axially magnetised permanent magnets are good candidates for applications in hybrid and electric vehicle drive-trains.

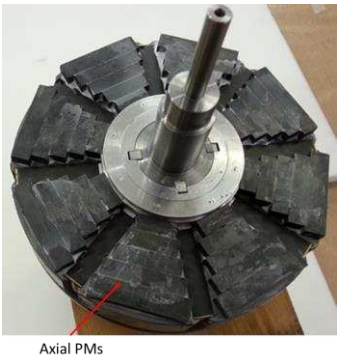

(a) Axial PMs

(b) Assembled rotor

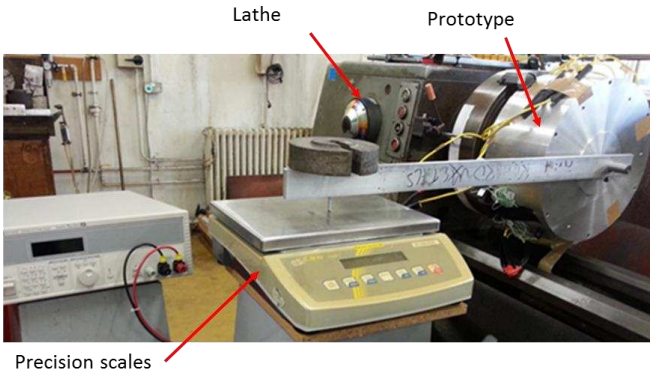

(c) Test set-up

Fig. 8 Prototype and set-up for static torque measurement.

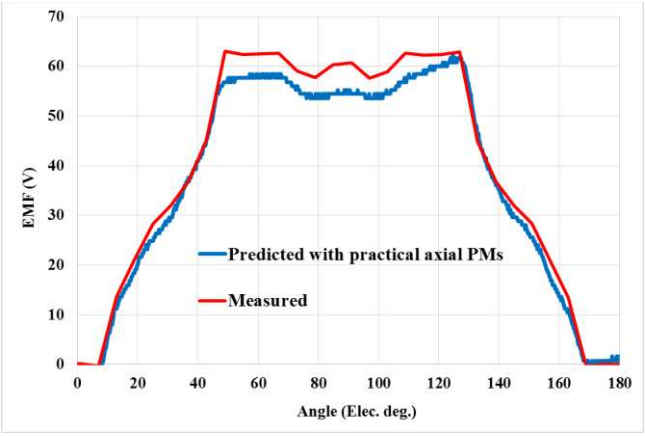

Fig. 9 EMF waveforms at 3000 rpm.

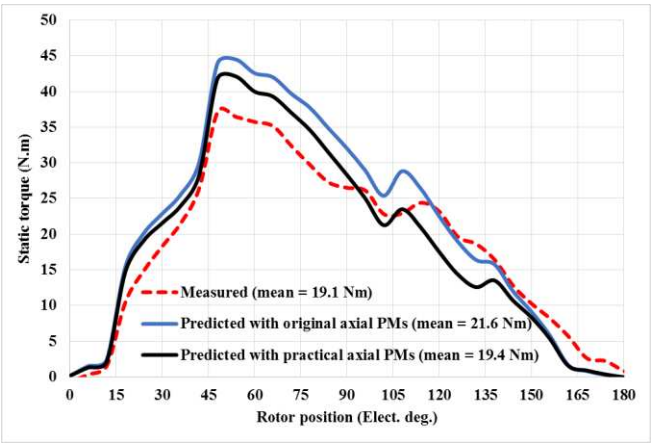

(a) DC current 36.7 A

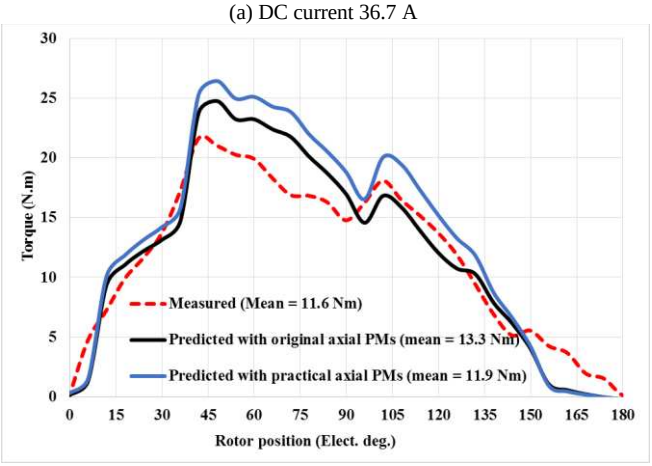

(b) DC current 22 A

Fig. 10 Static torque waveforms

VI. References

[1] T. Jahns, "Getting Rare-Earth Magnets Out of EV Traction Machines: A review of the many approaches being pursued to minimize or eliminate rare-earth magnets from future EV drivetrains," IEEE Electrification Magazine, vol. 5, pp. 6-18, 2017.

[2] H. Polinder, F. F. A. van der Pijl, G. J. de Vilder, and P. J. Tavner, "Comparison of direct-drive and geared generator concepts for wind turbines," Energy Conversion, IEEE Transactions on, vol. 21, pp. 725-733, 2006.

[3] A. Chiba, Y. Takano, M. Takeno, T. Imakawa, N. Hoshi, M. Takemoto, et al., "Torque Density and Efficiency Improvements of a Switched Reluctance Motor Without Rare-Earth Material for Hybrid Vehicles," Industry Applications, IEEE Transactions on, vol. 47, pp. 1240-1246, 2011.

[4] H. Kyu-Yun, R. Sang-Bong, Y. Byoung-Yull, and K. Byung-Il, "Rotor Pole Design in Spoke-Type Brushless DC Motor by Response Surface Method," Magnetics, IEEE Transactions on, vol. 43, pp. 1833-1836, 2007.

[5] K. Y. Hwang, J. H. Jo, and B. I. Kwon, "A Study on Optimal Pole Design of Spoke-Type IPMSM With Concentrated Winding for Reducing the Torque Ripple by Experiment Design Method," Magnetics, IEEE Transactions on, vol. 45, pp. 4712-4715, 2009.

[6] K. Atallah and J. Wang, "A Rotor With Axially and Circumferentially Magnetized Permanent Magnets," IEEE Transactions on Magnetics, vol. 48, pp. 3230-3233, 2012.

[7] "Ferrite Magnets FB Series," TDK Product Center, https://product.tdk.com/en/search/magnet/magnet/ferrite/info?part_no=FB6H, accessed on 22/10/2018.